Influence of the synthetic method on the properties of two-photon-sensitive mesoporous organosilica nanoparticles

Jonas G. Croissant, Olivier Mongin, Vincent Hugues, Mireille Blanchard-Desce, Xavier Cattoën, Michel Wong Chi Man, Vanja Stojanovic, Clarence Charnay, Marie Maynadier, Magali Gary-Bobo, et al.

Influence of the Synthetic Method on the Properties of Two-Photon-Sensitive Mesoporous Organosilica Nanoparticles.

Jonas Croissant*,[a] Olivier Mongin,[b] Vincent Hugues,[c] Mireille Blanchard-Desce*,[c] Xavier Cattoën,[d] Michel Wong Chi Man,[a] Vanja Stojanovic,[e] Clarence Charnay,[a] Marie Maynadier,[e,f] Magali Gary-Bobo,[e] Marcel Garcia,[e] Laurence Raehm,[a] and Jean-Olivier Durand*[a]

a) Institut Charles Gerhardt Montpellier, UMR-5253 CNRS-UM2-ENSCM-UM1cc 1701, Place Eugène Bataillon F-34095 Montpellier cedex 05, France. Fax: +33-467-143-852, E-mails: durand@um2.fr, jonasc@chem.ucla.edu

b) Institut des Sciences Chimiques de Rennes, CNRS UMR 6226 Université Rennes 1 Campus Beaulieu F-35042 Rennes Cedex, France.

c) Université Bordeaux, Institut des Sciences Moléculaires, UMR CNRS 5255, 351 Cours de la Libération, F-33405 Talence Cedex, France. E-mail: m.blanchard-desce@ism.u-bordeaux1.fr.

d) Institut NEEL, CNRS, and Université Grenoble Alpes, F-38042 Grenoble, France.

e) Institut des Biomolécules Max Mousseron UMR 5247 CNRS; UM 1; UM 2 - Faculté de Pharmacie, 15 Avenue Charles Flahault, 34093 Montpellier Cedex 05, France.

f) NanoMedSyn, Faculté de Pharmacie, Montpellier cedex 05, France.

Keywords: Mesoporous silica nanoparticles, two-photon, cancer cells, imaging, cross-section.

Abstract: Herein we report the modulation of the properties of mesoporous organosilica nanoparticles (NPs) via various synthetic approaches. Three types of elaborations were compared, one in aqueous media at 25 °C, and the other two at 80 °C in water or in a water/ethanol mixture. For all these methods, an alkoxysilylated two-photon photosensitizer (2PS) was co-condensed with tetraethylorthosilicate (TEOS) in the presence of cetyltrimethylammonium bromide (CTAB), leading to five two-photon-sensitive mesoporous

organosilica (M2PS) NPs. The M2PS NPs porous structure could be tuned from radial to wormlike and MCM-41 types of organization. Besides, the 2PS precursor spatial dispersion was found to be highly dependent of both the 2PS initial concentration and the elaboration process. As a result, two-photon properties were modulated by the choice of the synthesis, the best results being found in aqueous media at 25 or 80°C (Scheme 1). Finally, the M2PS NPs were used for *in-vitro* two-photon imaging of cancer cells.

Introduction :

Over the past few years, two-photon-sensitive NPs have attracted a lot of attention for theranostic nanomedicine.[1-16] Near-infrared (NIR) two-photon excitation is indeed very attractive for its deep-tissue penetration and 3D-spatiotemporal accuracy, which are crucial for site-specific cancer treatment.[17] Among various nanoplatforms, mesoporous silica nanoparticles (MSN) are particularly suited nanomedical devices for their low cytotoxicity, excretion[18, 19], selective endocytosis through the enhanced permeability and retention effect (EPR), and multifunctionality.[20-25] The diversity of MSN features arises from their large surface areas, tunable pore size, controllable shape and morphology, and known silicon chemistry.[26, 27] Besides, conversely to other non-porous inorganic NPs applied for two-photon nanomedicine, the sol-gel elaboration enables the co-condensation of versatile species with silica precursors to obtain organosilica NPs with high porosity.[28, 29]

Hence, two-photon fluorophores and photosensitizers (2PS) could be doped[8, 13, 30] or covalently bound in the material.[2, 31] Phase segregation, low doping efficiency of 2PS moieties, as well as the photosensitizer diffusion out of the nanomaterial often make the chemical grafting more attractive.[32] The 2PS concentration and spatial distribution in the NPs will be crucial for the final two-photon properties of each chromophore.[33] The control of many different parameters is thus required for the construction of efficient M2PS NPs.

Herein, we report a study on M2PS NPs designed from three different elaboration processes, in order to investigate the influence of the synthetic method on the properties of the M2PS NPs and on their two-photon properties (Scheme 1). The absorption and emission of

fluorescence, two-photon cross-sections and fluorescence quantum yields are systematically compared in five M2PS nanocarriers. It was found that the choice of the synthetic approach is crucial and can induce either the enhancement or the collapse of the two-photon absorption cross-sections of the M2PS NPs. Finally, the performances of the designed M2PS NPs is demonstrated for *in-vitro* fluorescence imaging.

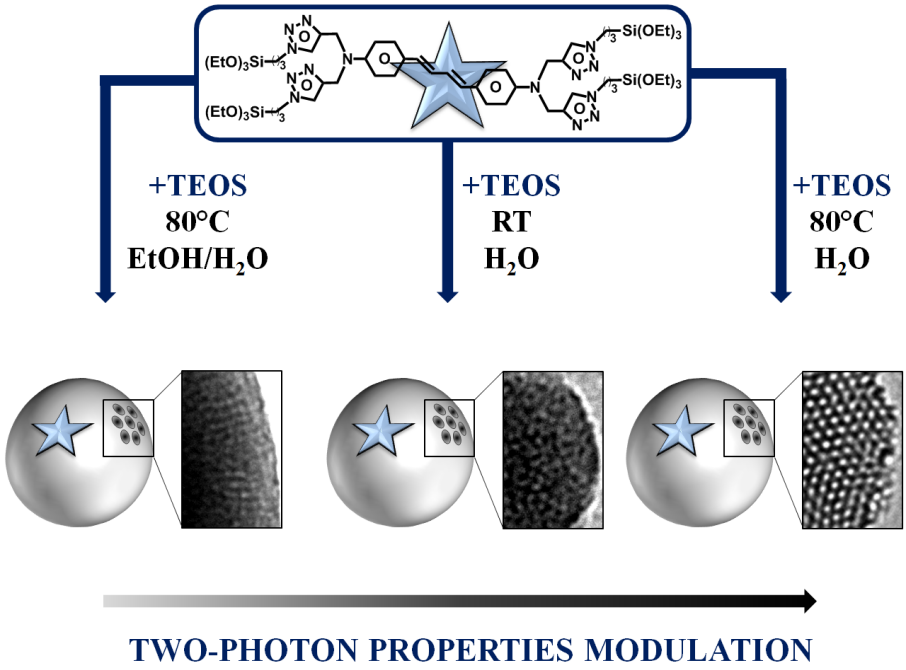

Scheme 1. Modulation of the two-photon properties of M2PS NPs via various synthetic pathways. Typical TEM images of the NPs porous framework are presented for each reaction.

Results and discussion

Firstly, the M2PS nanomaterials were designed via various synthetic approaches. Three procedures were compared which involved the co-condensation of a previously reported tetraalkoxysilylated two-photon photosensitizer (2PS)[2-4] with the TEOS silica precursor, through sodium hydroxide catalysis with a template of cetyltrimethylammonium bromide. The first approach involved modified Mann's conditions,[34] the six minutes reaction in aqueous media at 25°C. Two materials are compared from this procedure, **M2PS-1** and **M2PS-2**, with 9 and 18 weight percent (wt%) of 2PS respectively (see Table 1). In the second approach, the synthesis

was carried out at 80°C in a water/ethanol mixture (5:2, v:v) for 30 minutes; the related compound will be called **M2PS-3**. The third approach is a modified Lin's reaction,[35] which was performed in aqueous media at 80°C for 1 hour 30 minutes. Higher concentrations of 2PS precursor were used in this procedure, with 44 and 20 wt% of 2PS were obtained for **M2PS-4** and **M2PS-5** respectively.

Secondly, the structure and morphology of the M2PS nanomaterials were characterized. Transmission electron microscopy (TEM) images depicted nearly 80 nm nanospheres for all types of M2PS particles, except the 200 nm nanospheres obtained from the water/ethanol mixture for **M2PS-3** (Fig. 1A). Dynamic light scattering (DLS) size distributions showed that the best approaches to obtain monodisperse non-aggregated M2PS NPS were in aqueous media at 25°C for low 2PS concentration, or in aqueous media at 80°C for higher concentrations (Fig. 1B). Besides, electron micrographs revealed different types of porous frameworks for each reaction (see Scheme 1 and Fig. 1A). Typically, MCM-41 P6mm structure was obtained with the aqueous route at 25°C for **M2PS-1**, but the pore organization was very sensitive to the 2PS content. Comparing the same procedure in **M2PS-1** and **M2PS-2**, the increase of the 2PS content from 8 to 16 wt% led to an important structural disorganization, as testified with the small angle X-ray diffraction (XRD) patterns (Fig. 1C). Conversely, the third strategy performed at 80°C retained the MCM-41 hexagonal array of the pores for the **M2PS-4** and **M2PS-5** materials at high 2PS concentration, as displayed by TEM and XRD patterns, but enlargement of the Bragg peak and the TEM image for **M2PS-4** indicated a more slightly disordered structure. Alternatively, a radial porosity was obtained on **M2PS-3** NPs in the water/ethanol mixture (Fig. 1A, 1C). The mesoporous structure of the materials was validated by the nitrogen-adsorption-desorption technique. The BJH transform indicated pore diameters from 2.1 to 2.6 nm (see Table 2); high BET surface areas were found for all samples, ranging from 500 to 700 m^2/g (Fig. S1 to S5). Thus, both the size and the porosity of the M2PS nanomaterials make them suitable nanocarriers for nanomedicine applications.

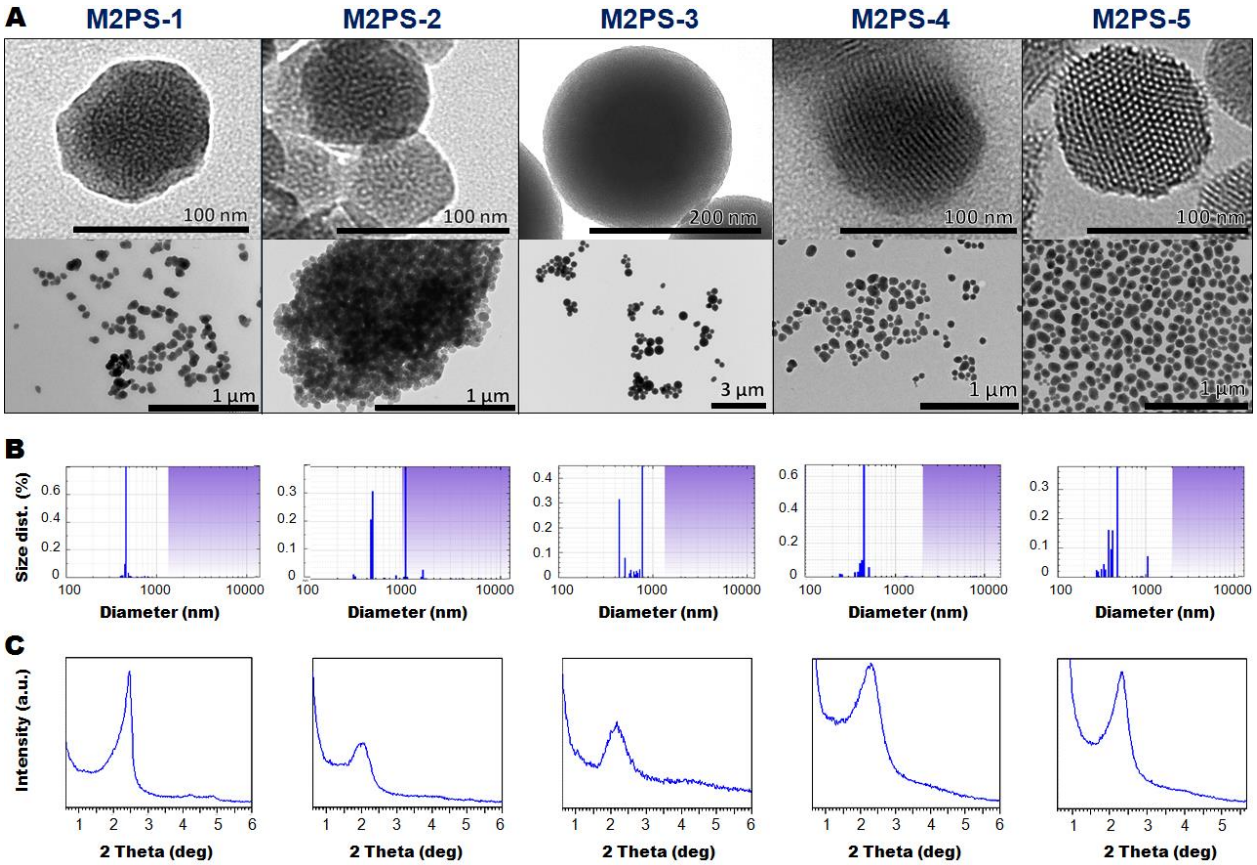

Figure 1. TEM images (A), DLS size distributions (B), and small angles XRD patterns of M2PS-1 to M2PS-5 NPs (C).

Table 1. 2PS weight per cent determination in M2PS NPs.

Sample	Method	NPs N wt% [a]	NPs 2PS wt% [b]	Reactant 2PS wt%
M2PS-1	25 °C/H_2O	1.3	7.7	8
M2PS-2	25 °C /H_2O	2.7	16.1	12
M2PS-3	80 °C/H_2O:EtOH	3.5	20.8	13
M2PS-4	80 °C/H_2O	7.3	43.5	38
M2PS-5	80 °C/H_2O	3.4	20.2	10

[a] Elemental analysis by combustion measurements of the NPs. [b] Determination based on the nitrogen wt% in the condensed 2PS moieties ($O_{1.5}$Si-R-Si$O_{1.5}$).

Thirdly, the efficiency of the 2PS encapsulation in the nanomaterials was found to be highly dependent on the synthetic route. UV-Visible spectroscopy demonstrated the successful encapsulation of the 2PS molecules in the silica framework of all M2PS NPs (Fig. S6 and S7). Solid state nuclear magnetic resonance (NMR) ^{29}Si and ^{13}C CPMAS spectra (Fig. S8) further supported that assertion. Besides, as shown in Table 1 with the comparison of the 2PS wt% in the NPs and in the reactants, the efficacy of the 2PS condensation was higher than that of TEOS. Interestingly, highly organically functionalized M2PS NPs could be designed with both syntheses at 80°C. However, the usefulness of the **M2PS-3** nanocarriers (water/ethanol mixture) is greatly impoverished, as we shall see with the photophysical properties.

Table 2. Textural properties of M2PS NPs.

Sample	**M2PS-1**	**M2PS-2**	**M2PS-3**	**M2PS-4**	**M2PS-5**
S_{BET} (m^2/g)	713	647	603	503	677
D_{pore} (nm)	2.0	2.3	2.3	2.5	2.6

The 2PS spatial distribution in the silica was then studied by absorption and emission of fluorescence, since this factor affects directly the photophysical properties of the NPs. The emission spectra (Fig. 2A) and the fluorescence quantum yields (Table 3) of the M2PS compounds were measured and compared to those of the 2PS molecular reference (2PS-Ref, see structure Fig. S9). The most fluorescent NPs were found to be **M2PS-1**, **M2PS-4**, and **M2PS-5**, the latter having a quantum yield two to four times larger than the formers. A bathochromic effect was also observed on the 2PS band, as seen in the normalized spectra (Fig. 2B). The most red-shifted band corresponds to the synthesis performed in the water/ethanol mixture, with an absorption maximum at 469 nm; then follows the aqueous mixture at 25°C (λ_{max} = 453-455 nm), and finally the aqueous reaction at 80°C ($\lambda_{max} \approx$ 448-450 nm). Such an observation was consistent with the absorption spectra of the M2PS NPs (Fig. S7). These results are the direct outcome of the spatial dispersion of the 2PS molecules in the mesoporous silica matrices, with an important aggregation[36] of the 2PS for the **M2PS-3** material. Thus we expected to obtain poorer two-photon properties on material having the most red-shifted 2PS emission bands. Indeed, the

aggregation of 2PS moieties via π-π stacking interactions or condensation generally leads to increased non-radiative de-excitation rates and therefore to a quenching of the fluorescence, as well as to a decrease of the two-photon absorption properties.[37]

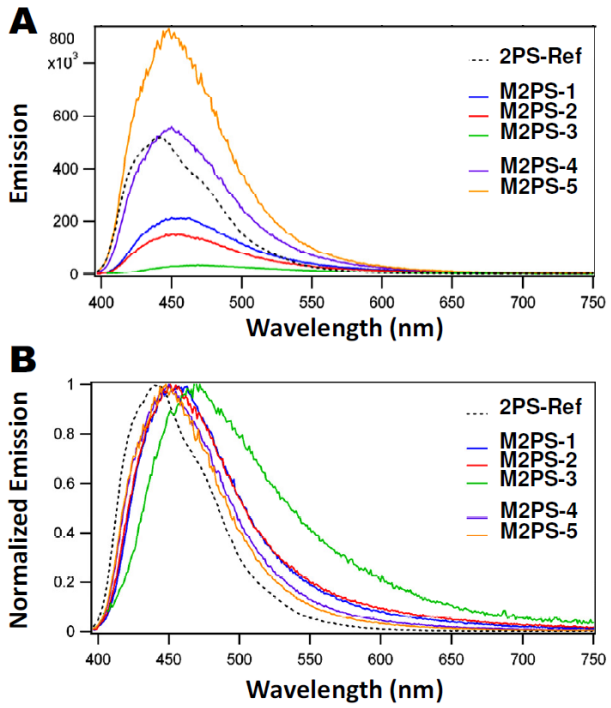

Figure 2. Fluorescence emission spectra of M2PS NPs (A), and the associated normalized spectra in ethanol (B).

Finally, the two-photon photophysical properties of the M2PS nanocarriers were investigated. The two-photon absorption cross-sections (σ_2) were determined between 700 and 900 nm by investigating their two-photon excited fluorescence, and as anticipated **M2PS-1**, **M2PS-4**, and **M2PS-5** displayed the highest cross-sections (see Table 3, and Fig. 3). It should be noticed that **M2PS-1**, **M2PS-4**, and **M2PS-5** also exhibit the largest quantum yields (11, 26, and 41%, respectively), while their maximum cross-sections ranged from 110 to 200 GM. In the case of the synthesis at 25°C, the increase of the 2PS concentration from 8% (**M2PS-1**) to 16% in **M2PS-2** leads to a decrease of both the fluorescence and the two-photon absorption cross-

section, from 11 to 8%, from 110 to 80 GM. On the other hand, comparing **M2PS-3** (reaction in water/ethanol) with **M2PS-5** (synthesis in water at 80°C), which both have 20% of photosensitizer, drastically different properties were obtained. Indeed, the latter exhibits a two-photon brightness (σ_2^{max} Φ_F) of 82 GM, which is 40 times larger than that of the former (2 GM, see Fig. 3B). Furthermore, for a given reaction, the 2PS threshold for optimum properties was different, in the first synthetic approach, 8% was the maximum, whereas in the third approach the 2PS content could be increased at least up to 25 % without quenching the properties. Consequently, the modulation of the two-photon properties of M2PS NPs could be done by an appropriate choice of the elaboration process.

Table 3. Photophysical properties of **M2PS** NPs in ethanol.

Sample	$\lambda_{abs}/\lambda_{em}$ (nm)	Φ_F [a]	σ_2^{max} [b] (GM)	σ_2^{max} Φ_F (GM)
M2PS-1	386/455	0.11	110	12
M2PS-2	388/453	0.08	80	6
M2PS-3	420/469	0.03	60	2
M2PS-4	385/450	0.26	180	46
M2PS-5	384/448	0.41	200	82

[a] Quinine bisulfate standard at 0.5 M in H_2SO_4. [b] Maximum two-photon absorption cross-section per chromophore. [c] Maximum two-photon action cross-section (two-photon brightness) per chromophore.

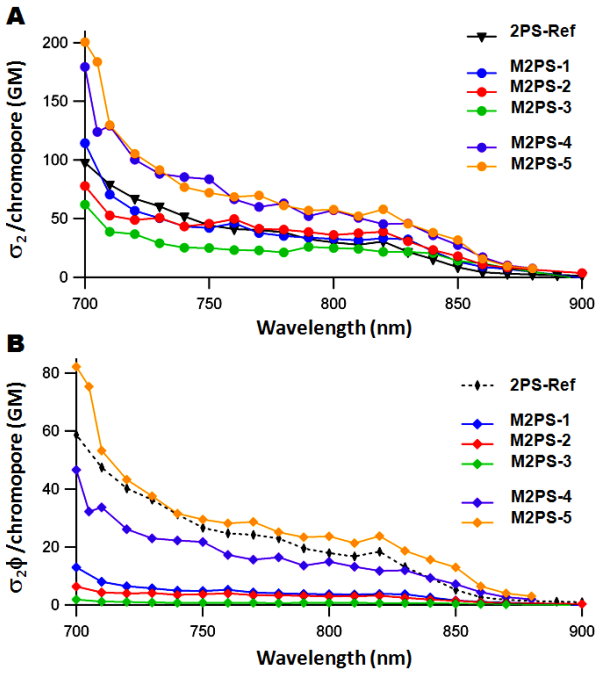

Figure 3. Two-photon absorption cross sections of M2PS NPs (A), and the corresponding two-photon brightness spectra in ethanol (B).

The two-photon potential of our M2PS NPs for fluorescence imaging was eventually tested *in vitro* on MCF-7 breast cancer cells. First, **M2PS-3 NPs** were found to have low cytotoxicity in cells up to 100 $\mu g.mL^{-1}$ (see Fig. S10). The two-photon laser excitation was then carried out using a Carl Zeiss two-photon confocal microscope at a low laser power (3% of the laser input) and at λ_{ex} = 760 nm. **M2PS-3 NPs** were incubated for 24 h with MCF-7 cancer cells at 40 $\mu g.mL^{-1}$ in 35 mm glass bottom dishes. In order to avoid artifact signals, we work on living cells without fixation or permeabilization of the membrane. The membranes of the cells were stained using a membrane marker (cell mask) for 15 min before imaging experiments. Two-photon confocal images correspond to a thin slice of cell (0.62 μm) without an out-of-focus signal, thus allowing us to determine which part of the signal is inside the cells (arrows). Even with the lowest two-photon absorption cross-section and quantum yield, **M2PS-3 NPs** were detected (Fig. 4), showing the successful endocytosis of these nanoparticles in cancer cells.

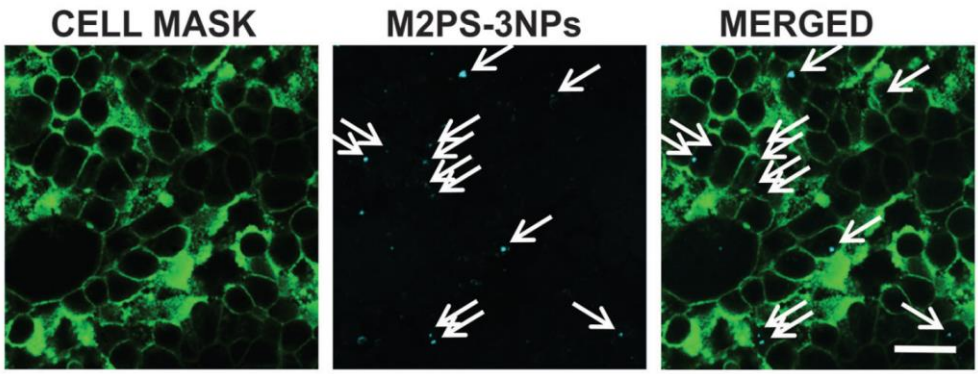

Figure 4. Two-photon *in vitro* imaging of **M2PS-3** NPs on living MCF-7 cells demonstrating the cellular uptake of the nanocarriers. Arrows pointed nanoparticles located inside the cells. Scale bar 20 μm.

Conclusions

In summary, we report a study of the properties of organically modified mesoporous silica NPs for two-photon excitation. The modulation of the two-photon properties was found to be highly dependent on the synthetic approach used, which directly affected the spatial distribution of the photosensitizers. Furthermore, the threshold of the photosensitizer maximum concentration varied according to the elaboration method, the best results being observed with a modified Mann's reaction in aqueous media at 25°C for low concentration, whereas the Lin's method at 80°C in water was preferred at higher concentrations. Hence, M2PS nanomaterial was used for *in-vitro* two-photon fluorescence imaging. This study highlights the intricacies implied in the design of efficient NIR two-photon-sensitive nanomaterials for various applications such as nanomedicine.

Experimental

Materials

Tetraethoxysilane, cetyltrimethylammonium bromide, sodium hydroxide, ammonium nitrate and tetrahydrofuran were purchased from Sigma-Aldrich. Absolute ethanol was purchased from Fisher Chemicals. R. Norma Pure.

Apparatus

Absorption spectra were recorded on a Hewlett-Packard 8453 spectrophotometer and fluorescence data were collected on an Edinburgh Instruments (FLS920) fluorimeter. Fluorescence quantum yields were measured in ethanol using quinine bisulfate in aqueous H_2SO_4 (0.5 M) as a reference (Φ_F = 0.546). Mass spectrometry was carried out at the Laboratoire de Spectrometrie de Masse (Lyon, France) with a Thermo-Finnigan MAT95 apparatus in electronic impact ionization mode. Dynamic light scattering analyses were performed using a Cordouan Technologies DL 135 Particle size analyzer instrument. ^{29}Si and ^{13}C CPMAS solid state NMR sequences were recorded with a VARIAN VNMRS300, using Q8MH8 and adamantane references respectively. TEM analysis performed on a JEOL 1200 EXII instrument. SEM analysis performed on a FEI Quanta FEG 200 instrument.

Synthesis

M2PS-1 NPs. A mixture of cetyltrimethylammonium bromide (345 mg, CTAB), and sodium hydroxide (20 mL, 0.2 M) was stirred at room temperature during 50 minutes at 700 rpm in a 250 mL three neck round bottom flask. Then, the stirring speed was changed to 1000 rpm. TEOS (1.6 mL) was added and after 40 seconds water (260 mL) was poured out. Afterwards, an ethanolic solution of the 2PS precursor (n_0 = 9.0 10^{-5} mol, in 1 mL EtOH) was added. The solution was then heated using a hair drier (from T_0=25 °C to T'=27 °C over 1-2 minutes), in order to trigger the condensation process. After 5 minutes 30 seconds of reaction, a solution of hydrochloric acid (0.2 M, *ca* 36 mL) was added to reach pH 6.9. Fractions were gathered in polypropylene tubes and collected by centrifugation for 15 minutes at 21 krpm. The sample was then extracted twice with an ethanolic solution of ammonium nitrate (6 $g.L^{-1}$), and washed three times with ethanol, water, and ethanol. Each extraction involved a sonication step of 30 minutes at 50 °C; the collection was carried out in the same manner. The as-prepared material was dried under air flow for few hours.

M2PS-2 NPs. A mixture of cetyltrimethylammonium bromide (345 mg, CTAB), and sodium hydroxide (20 mL, 0.2 M) was stirred at room temperature during 50 minutes at 700 rpm in a

250 mL three neck round bottom flask. Then, the stirring speed was changed to 1000 rpm, TEOS (1.6 mL) was added along with an ethanolic solution of the 2PS precursor (n_0 = 1.3*10^{-4} mol, in 1 mL EtOH). After 40 seconds, water (260 mL) was poured out. The solution was then heated using a hair drier (from T_0=25 °C to T'=27 °C over 1-2 minutes), in order to trigger the condensation process. After 5 minutes 30 seconds of reaction, a solution of hydrochloric acid (0.2 M, *ca* 36 mL) was added to reach a pH of 6.9. Fractions were gathered in polypropylene tubes and collected by centrifugation for 15 minutes at 21 krpm. The sample was then extracted twice with an ethanolic solution of ammonium nitrate (6 g.L^{-1}), and washed three times with ethanol, water, and ethanol. Each extraction involved a sonication step of 30 minutes at 50 °C in order to remove the CTAB surfactant; the collection was carried out in the same manner. The as-prepared material was dried under air flow for few hours.

M2PS-3 NPs. A mixture of cetyltrimethylammonium bromide (640 mg, CTAB), deionized water (100 mL), and ethanol (40 mL) was stirred at 80 °C for 40 minutes at 650 rpm in a 250 mL three neck round bottom flask. Then, an ethanolic solution of 2PS (n_0 = 9.0*10^{-5} mol, in 1 mL EtOH) was added to the stirred solution. A delay of 5 minutes was used to homogenize the solution, and TEOS (1.2 mL) was added via a syringe then the stirring speed was changed to 1000 rpm. The reaction was conducted for 30 minutes, then the solution was neutralized with hydrochloric acid (0.2 M), and the mixture was cooled down to room temperature. Fractions were gathered in polypropylene tubes and collected by centrifugation for 15 minutes at 21 krpm. The sample was then extracted twice with an ethanolic solution of ammonium nitrate (6 g.L^{-1}), and washed three times with ethanol, water, and ethanol. Each extraction involved a sonication step of 30 minutes at 50 °C; the collection was carried out in the same manner. The as-prepared material was dried under air flow for few hours.

M2PS-4 NPs. A mixture of cetyltrimethylammonium bromide (250 mg, CTAB), distilled water (120 mL), and sodium hydroxide (875 µL, 2 M) was stirred at 80 °C for 50 minutes at 700 rpm in a 250 mL three neck round bottom flask. Then, TEOS (1.0 mL) was added along with the two-photon photosensitizer (n_0 = 2.0*10^{-4} mol, in 1 mL of dry THF), and the condensation process was conducted for 1 hour 30 minutes. Afterwards, the solution was cooled to room temperature while stirring; fractions were gathered in polypropylene tubes and collected by centrifugation for 15 minutes at 21 krpm. The sample was then extracted twice with an ethanolic

solution of ammonium nitrate (6 $g.L^{-1}$), and washed three times with ethanol, water, and ethanol. Each extraction involved a sonication step of 30 minutes at 50 °C; the collection was carried out in the same manner. The as-prepared material was dried under air flow for few hours.

M2PS-5 NPs. A mixture of cetyltrimethylammonium bromide (250 mg, CTAB), distilled water (120 mL), and sodium hydroxide (875 µL, 2 M) was stirred at 80 °C during 50 minutes at 700 rpm in a 250 mL three neck round bottom flask. Then, TEOS (1.0 mL) was added along with the two-photon photosensitizer (n_0 = $6.4*10^{-5}$ mol, in 1 mL of dry THF), and the condensation process was conducted for 1 hour 30 minutes. Afterwards, the solution was cooled to room temperature while stirring; fractions were gathered in polypropylene tubes and collected by centrifugation for 15 minutes at 21 krpm. The sample was then extracted twice with an ethanolic solution of ammonium nitrate (6 $g.L^{-1}$), and washed three times with ethanol, water, and ethanol. Each extraction involved a sonication step of 30 minutes at 50 °C; the collection was carried out in the same manner. The as-prepared material was dried under air flow for few hours.

TPE fluorescence and measurements of the two-photon absorption cross-sections. Two-photon excited fluorescence spectroscopy was performed using a mode-locked Ti:sapphire laser generating 150 fs wide pulses at a 76 MHz rate, with a time-averaged power of several hundreds of mW (Coherent Mira 900 pumped by a 5 W Verdi). The laser light is attenuated using a combination of half-wave plates and a Glan-laser polariser and the excitation power is further controlled using neutral density filters of varying optical density mounted in a computer-controlled filter wheel. After five-fold expansion through two achromatic doublets, the laser beam is focussed by a microscope objective (10X, NA 0.25, Olympus, Japan) into a standard 1 cm stirred absorption cuvette containing the sample. The applied average laser power arriving at the sample was between 0.5 and 15 mW, leading to a time-averaged light flux in the focal volume on the order of 0.1-1 $mW/\mu m^2$. The generated fluorescence is collected in epifluorescence mode, through the microscope objective, and reflected by a dichroic mirror (675dcxru, Chroma Technology Corporation, USA). Residual excitation light is removed using a barrier filter (e650-2p, Chroma) and the fluorescence is coupled into a 600 µm multimode fiber by an achromatic doublet. The fiber is connected to a compact CCD-based spectrometer

(BTC112-E, B&WTek, USA), which measures the two-photon excited emission spectrum. The emission spectra are corrected for the wavelength-dependence of the detection efficiency using correction factors established through the measurement of reference compounds having known fluorescence emission spectra. Briefly, the set-up allows for the recording of corrected fluorescence emission spectra under multiphoton excitation at variable excitation power and wavelength. Absolute values for the two-photon excitation action cross sections $\sigma_2\Phi_F$ were obtained according to the method described by Xu *et al.* (*J. Opt. Soc. Am. B* **1996**, 13, 481). using 10^{-4} M fluorescein in 10^{-2} M aqueous NaOH as a reference, applying corrections for the refractive index of the solvent (M. H. V. Werts *et al.*, *Photochem. Photobiol. Sci.* **2005**, 4, 531). In the 700-720 nm excitation range, refined reference values for fluorescein were used. (C. Katan *et al.*, *J. Phys. Chem. B* **2007**, 111, 9468).

Two-photon imaging. The day prior to the experiment, MCF-7 human breast cancer cells (purchased from ATCC) were seeded onto bottom glass dishes (World Precision Instrument, Stevenage, UK) at a density of 10^6 cells.cm^{-2}. Then, adherent cells were washed once and incubated in 1 mL medium containing M2PS NPs at a concentration of 40 µg.mL^{-1} for 20 h. 15 minutes before the end of incubation, cells were loaded with Cell Mask (Invitrogen, Cergy Pontoise, France) for membrane staining at a final concentration of 5 µg.mL^{-1}. Before visualization, cells were washed gently with phenol red-free Dulbecco's modified Eagle's medium (DMEM). Cells were then scanned with a LSM 780 LIVE confocal microscope (Carl Zeiss, Le Pecq, France), at 760 nm with a slice depth (Z stack) of 0.62 µm.

Electronic Supplementary Information (ESI) available: [Characterization of the prepared MSN, photophysical properties]. See DOI: 10.1039/xxxxxx

Acknowledgements

We thank ANR P2N Mechanano for funding. Technological support from the Rio Imaging Platform is gratefully acknowledged.

References

1. M. Gary-Bobo, Y. Mir, C. Rouxel, D. Brevet, I. Basile, M. Maynadier, O. Vaillant, O. Mongin, M. Blanchard-Desce, A. Morère, M. Garcia, J.-O. Durand and L. Raehm, *Angew. Chem. Int. Ed.*, 2011, **123**, 11627-11631.
2. J. Croissant, A. Chaix, O. Mongin, M. Wang, S. Clément, L. Raehm, J.-O. Durand, V. Hugues, M. Blanchard-Desce, M. Maynadier, A. Gallud, M. Gary-Bobo, M. Garcia, J. Lu, F. Tamanoi, D. P. Ferris, D. Tarn and J. I. Zink, *Small*, 2014, **10**, 1752–1755.
3. J. Croissant, D. Salles, M. Maynadier, O. Mongin, V. Hugues, M. Blanchard-Desce, X. Cattoën, M. Wong Chi Man, A. Gallud, M. Garcia, M. Gary-Bobo, L. Raehm and J.-O. Durand, *Chem. Mater.*, 2014, **26**, 7214–7220.
4. J. Croissant, M. Maynadier, A. Gallud, H. Peindy N'Dongo, J. L. Nyalosaso, G. Derrien, C. Charnay, J.-O. Durand, L. Raehm, F. Serein-Spirau, N. Cheminet, T. Jarrosson, O. Mongin, M. Blanchard-Desce, M. Gary-Bobo, M. Garcia, J. Lu, F. Tamanoi, D. Tarn, T. M. Guardado-Alvarez and J. I. Zink, *Angew. Chem. Int. Ed.*, 2013, **125**, 14058-14062.
5. S. S. Banerjee and D.-H. Chen, *Nanotechnology*, 2009, **20**, 185103.
6. T. Zhao, K. Yu, L. Li, T. Zhang, Z. Guan, N. Gao, P. Yuan, S. Li, S. Q. Yao, Q.-H. Xu and G. Q. Xu, *ACS Appl. Mater. Interfaces*, 2014, **6**, 2700-2708.
7. S.-H. Cheng, C.-C. Hsieh, N.-T. Chen, C.-H. Chu, C.-M. Huang, P.-T. Chou, F.-G. Tseng, C.-S. Yang, C.-Y. Mou and L.-W. Lo, *Nano Today*, 2011, **6**, 552-563.
8. S. Kim, T. Y. Ohulchanskyy, H. E. Pudavar, R. K. Pandey and P. N. Prasad, *J. Am. Chem. Soc.*, 2007, **129**, 2669-2675.
9. J. Croissant, M. Maynadier, O. Mongin, V. Hugues, M. Blanchard-Desce, A. Chaix, X. Cattoën, M. Wong Chi Man, A. Gallud, M. Gary-Bobo, M. Garcia, L. Raehm and J.-O. Durand, *Small*, 2015, **11**, 295–299.
10. Z. Zhu, X. Zhao, W. Qin, G. Chen, J. Qian and Z. Xu, *Sci. China Chem.*, 2013, **56**, 1247-1252.
11. J.-L. Li, H.-C. Bao, X.-L. Hou, L. Sun, X.-G. Wang and M. Gu, *Angew. Chem. Int. Ed.*, 2012, **51**, 1830-1834.
12. T. M. Guardado-Alvarez, L. Sudha Devi, M. M. Russell, B. J. Schwartz and J. I. Zink, *J. Am. Chem. Soc.*, 2013, **135**, 14000-14003.
13. V. Lebret, L. Raehm, J. O. Durand, M. Smaihi, M. H. V. Werts, M. Blanchard-Desce, D.Methy-Gonnod and C. Dubernet, *J. Sol-Gel Sci. Technol.*, 2008, **48**, 32-39.
14. J. Park, A. Estrada, K. Sharp, K. Sang, J. A. Schwartz, D. K. Smith, C. Coleman, J. D.Payne, B. A. Korgel, A. K. Dunn and J. W. Tunnell, *Opt. Exp.*, 2008, **16**, 1590-1599.
15. C. Mauriello-Jimenez, J. G. Croissant, M. Maynadier, X. Cattoën, M. W. C. Man, J.Vergnaud, V. Chaleix, S. Vincent, M. Garcia and M. Gary-Bobo, *J. Mater. Chem. B*, 2015, 10.1039/C5TB00315F.
16. J. Lu, J. Croissant,J.-O. Durand, T. Guardado-Alvarez, J. I. Zink and F. Tamanoi, *Cancer Res.*, 2014, **74**, LB-9-LB-9.
17. M. Pawlicki, H. A. Collins, R. G. Denning and H. L. Anderson, *Angew. Chem. Int. Ed.*, 2009, **48**, 3244-3266.
18. Q. He, Z. Zhang, F. Gao, Y. Li and J. Shi, *Small*, 2011, **7**, 271-280.
19. J. S. Souris, C. H. Lee, S. H. Cheng, C. T. Chen, C. S. Yang, J. A. A. Ho, C. Y. Mou and L. W. Lo, *Biomaterials*, 2010, **31**, 5564-5574.

20. Z. Li, J. C. Barnes, A. Bosoy, J. F. Stoddart and J. I. Zink, *Chem. Soc. Rev.*, 2012, **41**, 2590-2605.
21. M. W. Ambrogio, C. R. Thomas, Y.-L. Zhao, J. I. Zink and J. F. Stoddartt, *Acc. Chem. Res.*, 2011, **44**, 903-913.
22. P. Yang, S. Gai and J. Lin, *Chem. Soc. Rev.*, 2012, **41**, 3679-3698.
23. S. Dib, M. Boufatit, S. Chelouaou, F. Sadi-Hassaine, J. Croissant, J. Long, L. Raehm, C. Charnay and J. O. Durand, *RSC Adv.*, 2014, **4**, 24838-24841.
24. J. Croissant and J. I. Zink, *J. Am. Chem. Soc.*, 2012, **134**, 7628-7631.
25. C. Argyo, V. Weiss, C. Bräuchle and T. Bein, *Chem. Mater.*, 2013, **26**, 435-451.
26. I. I. Slowing, J. L. Vivero-Escoto, B. G. Trewyn and V. S. Y. Lin, *J. Mater. Chem.*, 2010, **20**, 7924-7937.
27. K. K. Coti, M. E. Belowich, M. Liong, M. W. Ambrogio, Y. A. Lau, H. A. Khatib, J. I. Zink, N. M. Khashab and J. F. Stoddart, *Nanoscale*, 2009, **1**, 16-39.
28. B. G. Trewyn, I. I. Slowing, S. Giri, H.-T. Chen and V. S. Y. Lin, *Acc. Chem. Res.*, 2007, **40**, 846-853.
29. J. Kecht, A. Schlossbauer and T. Bein, *Chem. Mater.*, 2008, **20**, 7207-7214.
30. E. Chelebaeva, L. Raehm, J. O. Durand, Y. Guari, J. Larionova, C. Guerin, A. Trifonov, M. Willinger, K. Thangavel, A. Lascialfari, O. Mongin, Y. Mir and M. Blanchard-Desce, *J. Mater. Chem.*, 2010, **20**, 1877-1884.
31. T. M. Guardado-Alvarez, L. S. Devi, J.-M. Vabre, T. A. Pecorelli, B. J. Schwartz, J.-O. Durand, O. Mongin, M. Blanchard-Desce and J. I. Zink, *Nanoscale*, 2014, **6**, 4652-4658.
32. P. Couleaud, V. Morosini, C. Frochot, S. Richeter, L. Raehm and J. O. Durand, *Nanoscale*, 2010, **2**, 1083-1095.
33. X. Wang, A. R. Morales, T. Urakami, L. Zhang, M. V. Bondar, M. Komatsu and K. D. Belfield, *Bioconjugate Chem.*, 2011, **22**, 1438-1450.
34. C. E. Fowler, D. Khushalani, B. Lebeau and S. Mann, *Adv. Mater.*, 2001, **13**, 649-652.
35. H.-P. Lin and C.-P. Tsai, *Chem. Lett.*, 2003, **32**, 1092-1093.
36. K. Natte, T. Behnke, G. Orts-Gil, C. Würth, J. F. Friedrich, W. Österle and U. Resch-Genger, *J. Nanopart. Res.*, 2012, **14**, 1-10.
37. H. Y. Woo, B. Liu, B. Kohler, D. Korystov, A. Mikhailovsky and G. C. Bazan, *J. Am. Chem. Soc.*, 2005, **127**, 14721-14729.
35. H.-P. Lin and C.-P. Tsai, *Chem. Lett.*, 2003, **32**, 1092-1093.
36. K. Natte, T. Behnke, G. Orts-Gil, C. Würth, J. F. Friedrich, W. Österle and U. Resch-Genger, *Journal of Nanoparticle Research*, 2012, **14**, 1-10.
37. H. Y. Woo, B. Liu, B. Kohler, D. Korystov, A. Mikhailovsky and G. C. Bazan, *J. Am. Chem. Soc.*, 2005, **127**, 14721-14729.